

Research Article

Parameter Optimization in Resistance Spot Welding of AISI 1060 Steel Using Adaptive Neural Fuzzy Inference System and Sensitivity Analysis

M. Safari*, A.H. Rabiee and V. Tahmasbi

Department of Mechanical Engineering, Arak University of Technology, Arak, 38181-8411, Iran

ARTICLE INFO

Article history:

Received 3 August 2021

Reviewed 2 October 2021

Revised 12 October 2021

Accepted 13 October 2021

Keywords:

Resistance spot welding

AISI 1060 steel

Adaptive neural-fuzzy inference system

Gray wolf optimization algorithm

Sobol sensitivity analysis method

ABSTRACT

Resistance spot welding process of AISI 1060 steel has been experimentally investigated by studying the effects of welding current, electrode force, welding cycle and cooling cycle on tensile-shear strength. Using the response surface methodology, experimental tests are performed. An adaptive neural-fuzzy inference system is applied to model and predict the behavior of tensile-shear strength. Additionally, the optimal parameters of adaptive neural-fuzzy inference systems are obtained by the gray wolf optimization algorithm. For modeling the process behavior, the results of experiments have been employed for training (70% of data) and testing (30% of data) of the inference system. The results show that the applied network has been very successful in predicting the tensile-shear strength and the coefficient of determination and mean absolute percentage error for the test section data are 0.96 and 6.02%, respectively. This indicates the considerable accuracy of the employed model in the approximation of the desired outputs. After that, the effect of each input parameter on tensile-shear strength is quantitatively evaluated with the Sobol sensitivity analysis method. The results show that the tensile-shear strength of the joint rises by increasing the welding current and welding cycle and also decreasing the electrode force and cooling cycle.

© Shiraz University, Shiraz, Iran, 2021

1. Introduction

High carbon steels with high strength and suitable wear resistance are used as tool materials. In recent years, some researchers have proposed methods and materials for welding these types of steels but there are still many problems in this regard due to transforming the heat affected zone to a very hard martensite phase that decreases the ductility of weld metal. Resistance spot welding (RSW) is widely employed in many industries for the purpose of joining sheet metals. It is

employed in fabrication of automobiles, buses, office furniture, airplanes, aeronautics and many other industries [1-5]. The RSW contains thermal, mechanical, electromagnetic, fluid flow and metallurgical phenomena and hence is very complicated for investigation [6]. In RSW, two or more parent sheet metals are pressed by electrode force. Then, a welding current is applied to the electrodes and therefore, a heat energy is generated between the sheet metals due to their electrical resistance. Hence, the generated heat leads to creating a weld nugget that is produced at the faying

* Corresponding author

E-mail address: m.safari@arakut.ac.ir (M. Safari)<https://doi.org/10.22099/IJMF.2021.41376.1192>

surface of sheets. The key parameter for integrity of the structures fabricated by RSW especially in load-bearing conditions is the mechanical strength of the joints. However, controlling the welding parameters is very important in achieving the welded joints with proper strength. In recent years, many research studies have been conducted in this field. The effects of process parameters on mechanical properties of welded joints of stainless steel 304 were studied by Kumar et al. [7]. It was concluded that welding time had a considerable effect on tensile shear tensile (TSS). In addition, the electrode force and welding time had important effects on microhardness. Chen et al. [8] designed a novel slightly concave electrode to reduce the unfavorable interfacial fracture mode. Their results showed that by the proposed electrode, the range of welding current that leads to the pullout failure mode is doubled. Zhao et al. [9] optimized the process parameters of RSW with entropy weight method. In their method, the nugget diameter, TSS and failure energy were converted into a welding quality index. Their results showed that the welding current and welding time are the most important parameters that affect the weld quality, respectively. Xia et al. evaluated the expulsion intensity in a RSW process [10] by calculating the percentage of ejected metal from the melt during the expulsion. They concluded that the rapid decreasing in signals of force and displacement showed the amount of expelled metal in RSW. Ordoñez et al. [11] studied the microhardness, TSS and fatigue behavior of RSW joints for DP980 steel sheets. Their results showed that the stress concentration near the fusion zone leads to a decrease in fatigue life of the welds. The optimization of RSW process of TRIP and DC05 steels was performed with Valera et al. [12] by Taguchi design of the experiment method. They concluded that the most effective parameters on TSS of the joints are welding time and current, respectively. Vignesh et al. [13] studied the effects of heating cycle, electrode tip diameter and welding current on TSS of the joints of AISI 316L and 2205 Duplex sheets with Taguchi method and concluded that the welding current has the most considerable effect of TSS. Wan et al. [14]

compared back propagation neural network (BPNN) and probabilistic neural network (PNN) for predicting the weld quality in small scale RSW. The results indicated that in estimation of failure load and quality level classification, the BPNN and PNN methods were more proper, respectively. Artificial intelligence (AI) is widely used to detect the relationship between input and output parameters extracted from a dynamic resistance signal compared to mathematical modeling. Artificial neural network (ANN) is used to find the correlation between input and output parameters and is more practical than traditional techniques [15]. Adaptive neural-fuzzy inference system (ANFIS) is a mixture of fuzzy systems and artificial neural network which utilize the learning ability of artificial neural networks to attain the fuzzy system parameters [16].

In this paper, the ANFIS method is utilized to model the influence of main parameters in RSW for predicting the TSS of the joints. For this purpose, with response surface methodology (RSM), the welding tests are administered and the results of joints strength will be used to train and test the ANFIS. In addition, to obtain the optimal structure of the ANFIS, the gray wolf optimization (GWO) algorithm is employed. Then, with the Sobel statistical sensitivity analysis method, the sensitivity of TSS variations based on changes in each of the input parameters is investigated.

2. Materials and Methods

2.1. Optimized intelligent modeling

2.1.1. Optimized intelligent modeling

Fuzzy logic and neural network methods are used in the ANFIS. The ANFIS consists of antecedent and sequential parts which are interconnected in the if-then rules. Takagi-Sugeno (TS) fuzzy model is a type of ANFIS network that has 2 inputs and 1 output as is shown in Fig. 1.

As shown in Fig. 1, there are 2 inputs (x and y), and 1 output (f) in the ANFIS with the rules in the form of: Rule one: If (x equals A_1) and (y equals B_1), then it becomes $f_1 = p_1x + q_1y + r_1$

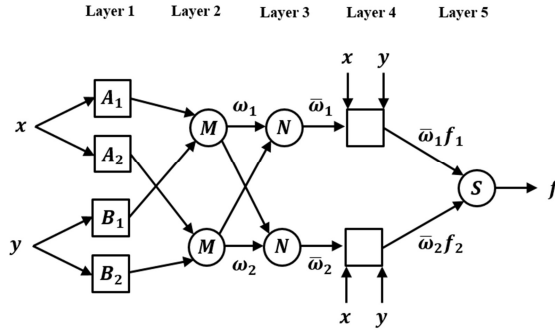


Fig. 1. ANFIS network structure.

Rule two: If (\$x\$ equals \$A_2\$) and (\$y\$ equals \$B_2\$), then it becomes \$f_2 = p_2x + q_2y + r_2\$

In this system, \$A_i\$ and \$B_i\$ are fuzzy sets and \$f\$ is the output of the system. Also, \$p_i, q_i, r_i\$, are constants that are attained throughout the learning section [17]. If output of every single layer is considered to be \$O_i^j\$ (output of node \$i\$ in layer \$j\$), then the functions and operations of the distinct layers can be explained as:

Layer one: Every single node is identical to a fuzzy set and the output of that node in the corresponding set is identical to the degree of membership of the input variable, in this layer. The parameters of node specify the form of the membership function (MF) in the node. Since Gaussian MFs are used in present the paper, it drives:

$$\mu_{Ai}(x) = e^{-\frac{1}{2}(\frac{x-c_i}{\sigma_i})^2} \quad (1)$$

where \$\sigma_i\$ and \$c_i\$ the width and center of Gaussian MFs and \$x\$ is the input value of each node.

Layer two: The values of the inputs of every single node are multiplied by each other and the rule firing strength is calculated as:

$$O_i^2 = \omega_i = \mu_{Ai}(x)\mu_{Bi}(y), \quad i = 1,2 \quad (2)$$

where \$\mu_{Ai}\$ is degree of MF, \$x\$ in \$A_i\$ and \$\mu_{Bi}\$ is degree of MF \$y\$ in \$B_i\$.

Layer three: The nodes compute the associated weight of the rules, where \$\omega_i^n\$ is normalized fire intensity of rule \$i\$.

$$O_i^3 = \omega_i^n = \frac{\omega_i}{\omega_1 + \omega_2} \quad i = 1,2 \quad (3)$$

Layer four: the fourth layer is known as the rule layer that is obtained by multiplying the normalized fire intensity (obtained in the third step) by the output of the TS fuzzy system.

$$O_i^4 = \omega_i^n f_i = \omega_i^n (p_i x + q_i y + r_i), \quad i = 1,2 \quad (4)$$

Layer five: the fifth layer, which is the last step, consists of a node where all the inputs are gathered together:

$$O_i^5 = \sum_{i=1}^2 \omega_i^n f = \frac{\omega_1 f_1 + \omega_2 f_2}{\omega_1 + \omega_2}, \quad i = 1,2 \quad (5)$$

Recently, various optimization techniques such as particle swarm algorithm and genetic algorithm have been used to increase the performance of the ANFIS system. GWO is one of the newest and most efficient optimization methods that is utilized here to optimize the ANFIS network.

2.1.2. Gray wolf optimization algorithm

In the Gray Wolf Optimization algorithm (GWO), which is inspired by Canadian Gray Wolf hunting actions, by Mirjalili et al. [18] it has been suggested that they fall into the category of population-based optimization algorithms. Gray wolves have a leading social hierarchy, as revealed in Fig. 2. The pioneers of the crowd are a male and a female known as Alpha. The next layer in the gray wolf hierarchy is Beta. Beta ones are secondary wolves that aid with Alpha in decisions or other group actions. Delta wolf must report to Alpha and

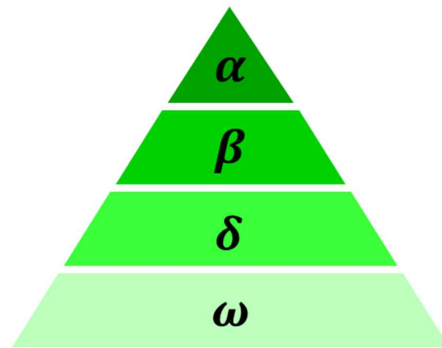


Fig. 2. The hierarchy of Gray wolves.

Beta but dominates Omega. Omega has the lowest rank, meaning it should always obey other wolves. The GWO algorithm, like the Particle Swarm optimization algorithm, starts from a random population. In each iteration, the Alpha, Beta, and Delta crowd renew their location according to their prey location. This update also endures until the space among the wolves and the prey is stopped or a satisfactory result is achieved. In GWO, Alpha wolves are the finest result. Other crowd tracks along with its dominion. Hunting action is done mainly by Alpha and Beta wolves and henceforth by the Delta followed by Omega [18]. Specifically, the GWO consists of the following steps:

Step one: The initial population of gray wolves is randomly created. The created crowd is characterized by the n-dimensional search space for operating M locations. To repeat, start with $k = 0$ initialization and continue to k_{max} .

$$P_j(k) = [P_j^1(k) \dots \dots P_j^f(k) \dots \dots P_j^n(k)]^T \quad (6)$$

$, j \in \{\alpha, \beta, \delta\}$

where $k = 1, 2, \dots, k_{max}$ are the present iteration numbers, k_{max} is the maximum repetition, and $P_\alpha(k), P_\beta(k), P_\delta(k)$ is the solutions vector.

Step two: The performance of every single member of the population is assessed based on the accuracy of the approximation of the experimental data of the present problem. Evaluating the performance of each member leads to the value of the fit function (objective function) that is used for the GWO optimization algorithm using:

$$P_i(k) = \rho, i = 1, 2, \dots, M$$

Step three: The finest 3 solutions obtained so far, we mean $P_\alpha(k), P_\beta(k), P_\delta(k)$, are identified by:

$$J(P_\alpha(k)) = \min_{i=j, \dots, M} \{J(P_i(k)), P_i(k) \in D_p\} \quad (7)$$

$$J(P_\beta(k)) = \min_{i=j, \dots, M} \{J(P_i(k)), P_i(k) \in D_p/P_\alpha(k)\} \quad (8)$$

$$J(P_\delta(k)) = \min_{i=j, \dots, M} \{J(P_i(k)), P_i(k) \in D_p/P_\alpha(k), P_\beta(k)\} \quad (9)$$

Eq. (10) has one situation for the outcome:

$$J(P_\alpha(k)) < J(P_\beta(k)) < J(P_\delta(k)) \quad (10)$$

Step four: Search vector constants are obtained utilizing Eq. (11) and (12):

$$R_j(k) = [r_j^1(k) \dots r_j^f(k) \dots r_j^n(k)]^T \quad (11)$$

$$S_j(k) = [s_j^1(k) \dots s_j^f(k) \dots s_j^n(k)]^T \quad (12)$$

$, j \in \{\alpha, \beta, \delta\}$

in which:

$$r_j^f(k) = r^f(k)(2q^f - 1), \quad (13)$$

$$s_j^f(k) = 2q^f, j \in \{\alpha, \beta, \delta\} \quad (14)$$

where q^f the uniform distribution of a random number in the range $0 \leq q^f \leq 1, f = 1 \dots n$ and the constant $r^f(k)$ in the search process is reduced from 2 to 0.

$$r^f(k) = 2[1 - (k - 1)/(k_{max} - 1)] \quad (15)$$

$, f = 1 \dots n$

Step five: Search constants factors are permitted to discover their new location by using Eq. (16).

$$V_j^i(k) = |S_j^f(k)P_j^f(k) - P_i^f(k)| \quad (16)$$

$, i = 1 \dots M, j \in \{\alpha, \beta, \delta\}$

By utilization of notation $P^j(k)$ for renewed Alpha, Beta and Delta solutions:

$$P^j(k) = [p^{j1}(k) \dots p^{jf}(k) \dots x^{jm}(k)]^T \quad (17)$$

$, j \in \{\alpha, \beta, \delta\}$

The components of these solutions are as follows:

$$P^{if}(k) = p_j^f(k) - r_j^f(k)v_j^i(k) \quad (18)$$

$, f = 1 \dots n, i = 1 \dots M, j \in \{\alpha, \beta, \delta\}$

And the renewed solution vector $P_i(k + 1)$ is calculated by Eq. (19):

$$P_i(k + 1) = (P^\alpha(k) + P^\beta(k) + P^\delta(k))/3 \quad (19)$$

$, i = 1 \dots M$

Step six: The updated solution $P_i(k + 1)$ is validated by the objective function.

Step seven: The GWO is recurrent from step two till the repetition k reaches the maximum value from the initial value.

Step eight: In the last level, the algorithm stops, and the finest solution ever found is saved as:

$$\rho^* = \arg \min_{i=1...M} J(P_i(k_{max})) \quad (20)$$

2.1.3. Sensitivity analysis

Sensitivity analysis is a useful utensil in evaluating of the systems and extracted the influence of the input parameters on output of system for engineering problems. Sensitivity analysis describes the output uncertainty of the model and shows how this uncertainty is related to the inputs of the system [19].

2.1.4. Sobol sensitivity analysis

In this method, with function of $Y = f(x)$ that is the output and $X(x_1, x_2, \dots, x_n)$ as the input vector, the output variance of the model (V) is defined as the summation of the each decomposed term as presented in Eq. (21):

$$V(Y) = \sum_{i=1}^n V_i + \sum_{i < j \leq n} V_{ij} + \dots + V_{1, \dots, n} \quad (21)$$

where V_i is the first-order effect for each input parameter $[x_i (V_i = V[E(Y|x_i)])]$ and $V_{ij} = V[E(Y|x_i, x_j)] - V_i -$

$V_j]$ to $V_{1, \dots, n}$ shows the interaction effects between input parameters. Sensitivity index is ratio of each order variance to total variance, so that $S_i = \frac{V_i}{V}$ is first order sensitivity index, $S_{ij} = \frac{V_{ij}}{V}$ is second order sensitivity index and so forth. Total sensitivity index as the total effect of each parameter is defined as the summation of all orders of the parameter. It is computed by the following equation [19].

$$S_{Ti} = S_i + \sum_{i \neq j} S_{ij} + \dots \quad (22)$$

2.2. Resistance spot welding process

For performing the RSW experiments, a constant alternating current welder (Messer Griesheim) with capacity of 150 kVA was used. In this welding machine, the RSW process was controlled by a microcomputer with fully digital control. During the entire period of experiments, the water was circulated in the electrodes in order to improve the heat transfer. AISI 1060 steel sheets with thickness of 1 mm were used in the RSW experiments. In Table 1, the chemical composition of AISI 1060 sheets is presented.

In Fig. 3, a schematic of the RSW welded specimens with the corresponding dimensions is shown. It should be noted that the dimensions of welded steel sheets are length = 150 mm, width = 25 mm and thickness = 1 mm

Table 1. Chemical composition (%) of the AISI 1060 steel sheets used in the RSW experiments

Elements	C	Si	Mn	P	S	Cr	Mo
Weight %	0.62	0.42	0.71	≤ 0.03	≤ 0.05	0.21	0.08

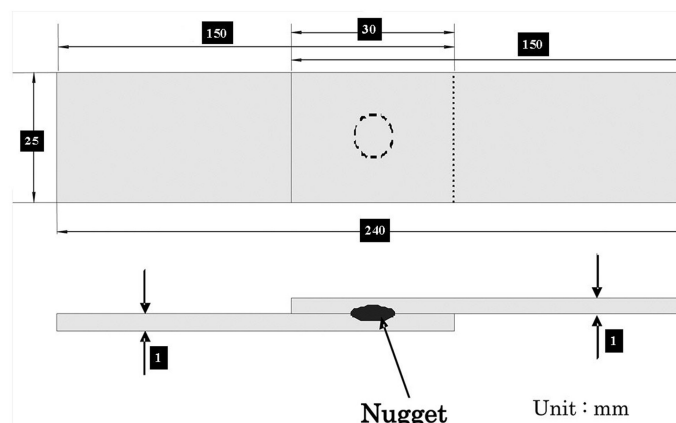


Fig. 3. Schematics of the RSW welded specimens with the corresponding dimensions.

as presented in Fig. 3. Additionally, with a dry air jet, the sheet surfaces were cleaned. Some trial experiments were performed in order to determine the limits of process parameter. As can be seen in Fig. 3, the sheets with overlaps of 30 mm were placed between the centers of electrodes. RSM is an optimization technique for

obtaining the optimum values of input parameters for achieving the best output. 31 experiments were designed based on RSM and design matrix (Table 2). The performed experiments are presented in Table 3.

In Fig. 4, the welded specimens by RSW according to experiments in Table 3 are presented.

Table 2. Coded and actual values of parameters for the RSW investigations

Parameter	Limits				
	-2	-1	0	+1	+2
Welding current (kA)	6.4	7.8	9.2	10.6	12
Welding cycle (cycle)	20	25	30	35	40
Cooling cycle (cycle)	0	12.5	25	37.5	50
Electrode force (N)	800	1100	1400	1700	2000

Table 3. Design layout of RSW experiments based on response surface methodology

Sample	Welding current (kA)	Welding cycle	Cooling cycle	Electrode force (N)
1	7.8	25	12.5	1100
2	10.6	25	12.5	1100
3	7.8	25	12.5	1700
4	10.6	25	12.5	1700
5	7.8	35	12.5	1100
6	10.6	35	12.5	1100
7	7.8	35	12.5	1700
8	10.6	35	12.5	1700
9	7.8	25	37.5	1100
10	10.6	25	37.5	1100
11	7.8	25	37.5	1700
12	10.6	25	37.5	1700
13	7.8	35	37.5	1100
14	10.6	35	37.5	1100
15	7.8	35	37.5	1700
16	10.6	35	37.5	1700
17	6.4	30	25	1400
18	12	30	25	1400
19	9.2	30	25	800
20	9.2	30	25	2000
21	9.2	20	25	1400
22	9.2	40	25	1400
23	9.2	30	0	1400
24	9.2	30	50	1400
25	9.2	30	25	1400
26	9.2	30	25	1400
27	9.2	30	25	1400
28	9.2	30	25	1400
29	9.2	30	25	1400
30	9.2	30	25	1400
31	9.2	30	25	1400



Fig. 4. The welded specimens by RSW and according to Table 3 experiments.

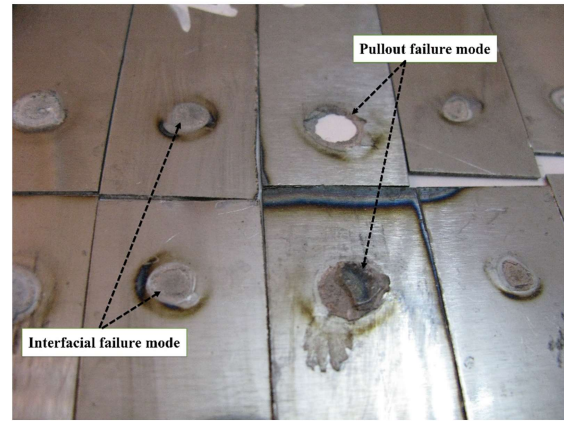


Fig. 5. Some of the RSW joints after tensile-shear test

With a Kpruf universal testing machine, the tensile-shear tests were conducted for evaluating the strength of the weld. As it is seen in Fig. 5, during the tensile-shear test, interfacial and pullout failure modes have been observed.

As the reliability of 95% is sufficient in engineering investigations, the parameters with p-value less than 0.05 influence the desired output [20]. Hence, based on Table 4, the welding current, welding cycle, cooling cycle and electrode force, their squares and some interactions influence the TSS of the spot welds. The R-sq= 95.77 % and R-sq (adj) = 93.66% for TSS of joints prove the suitable accuracy of the proposed model.

2.3. Analysis of variance (ANOVA)

ANOVA results of TSS include the effects of process parameters and their interactions are presented in Table 4 for the designed experiments in Table 3.

As the reliability of 95% is sufficient in engineering investigations, the parameters with p-value less than 0.05 influence the desired output [20]. Hence, based on Table 4, the welding current, welding cycle, cooling cycle and electrode force, their squares and some interactions influence the TSS of the spot welds. The R-sq= 95.77 % and R-sq (adj) = 93.66% for TSS of joints prove the suitable accuracy of the proposed model.

Table 4. ANOVA for TSS of RSW joints

Source	DF	Adj SS	Adj MS	F-Value	P-Value
Model	10	27771450	2777145	45.28	0.000
Linear	4	20701667	5175417	84.39	0.000
Welding current (kA)	1	11070417	11070417	180.51	0.000
Welding cycle	1	3760417	3760417	61.32	0.000
Cooling cycle	1	1450417	1450417	23.65	0.000
Electrode force (N)	1	4420417	4420417	72.08	0.000
Square	4	5998533	1499633	24.45	0.000
Welding current (kA)*Welding current (kA)	1	2944240	2944240	48.01	0.000
Welding cycle*Welding cycle	1	1908984	1908984	31.13	0.000
Cooling cycle*Cooling cycle	1	1241631	1241631	20.25	0.000
Electrode force (N)*Electrode force (N)	1	1728742	1728742	28.19	0.000
2-Way Interaction	2	1071250	535625	8.73	0.002
Welding current (kA)*Welding cycle	1	680625	680625	11.10	0.003
Welding cycle*Cooling cycle	1	390625	390625	6.37	0.020
Error	20	1226553	61328		
Pure Error	6	33220	5537		
Total	30	28998003			

3. Results and Discussion

3.1. The results of ANFIS-GWO system

In the present study, there is 31 empirical data for ANFIS construction, involving four inputs (mentioned process parameters) and single output (TSS). This data collection is arbitrarily separated into 2 subsets, 70% for training and 30% for testing. The parameters of the input and output membership functions (as well as the if-then fuzzy rules) are optimized by the aid of GWO algorithm. Figs. 6, 7, 8 and 9 show the optimized Gaussian membership functions associated with input process parameters. It should be noted that the degree of membership functions has been provided in a normalized form.

Also, Fig. 10 shows the actual experimental data and has also predicted data attained by ANFIS for both the training and testing phases. It is shown that the accuracy of the ANFIS predicted data is very high for the training section if the ANFIS is trained based on the data of this section. In addition, the ANFIS has been able to predict

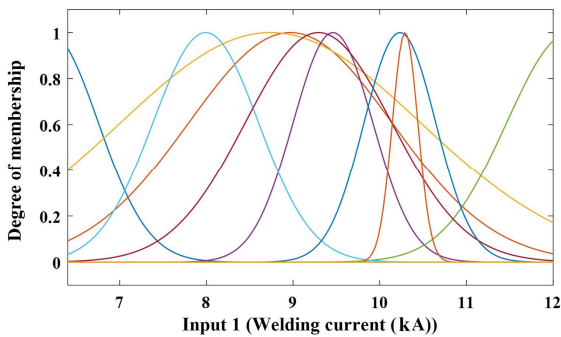


Fig. 6. The optimized membership function for welding current.

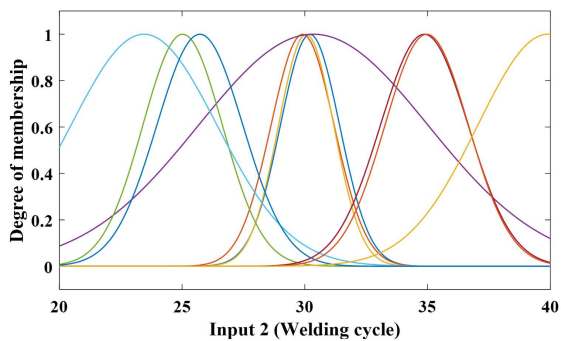


Fig. 7. The optimized membership function for welding cycle.

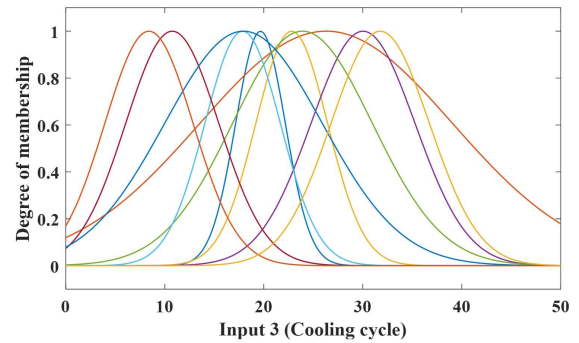


Fig. 8. The optimized membership function for cooling cycle.

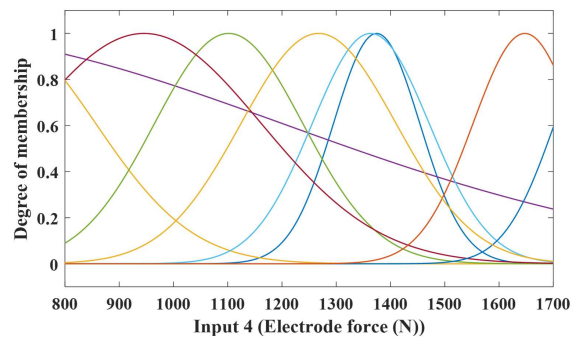


Fig. 9. The optimized membership function for electrode force.

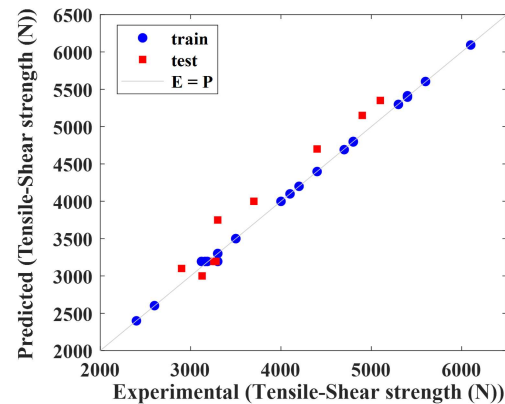


Fig. 10. Comparison between experimental and predicted data.

the data of the test section appropriately. Next, Fig. 11 shows the value of the TSS of welds for the actual and predicted data in both the training and testing sections. As can be seen in these diagrams, the actual experimental data and ANFIS predicted data in the training phase coincide quite well. The second part of the

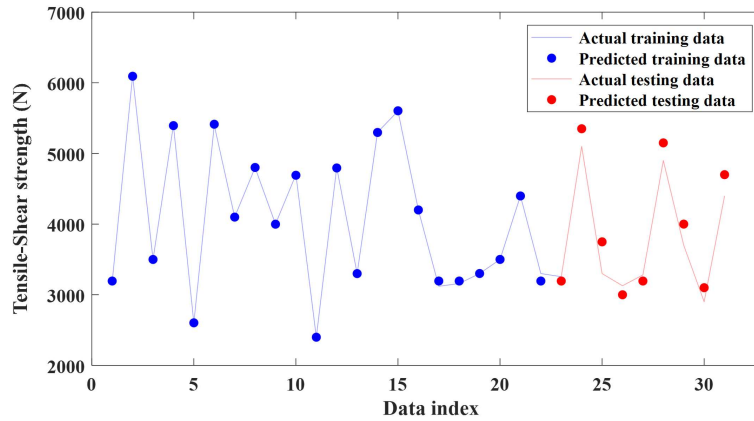


Fig. 11. Differences between experimental and test data for prediction of TSS.

diagrams (test section) also show that the ANFIS has been able to predict the data related to the test section. Moreover, Fig. 12 illustrates the error histogram for both training and testing phases. The y-axis in Fig. 12 (error distribution) represents the number. It can be seen here that the error frequency is greater at values closer to zero especially for the training part.

Moreover, Fig. 13 demonstrates the error and mean absolute percentage error (MAPE) associated with the

training and testing sections. As can be seen, the amount of error in the test section is greater than the training section. It can also be seen that the MAPE for the test section is close to zero and for only three data index the MAPE has been increased to a maximum of 2%. Furthermore, the network MAPE for the test section is low and except for one data, the rest of the values did not exceed 8%.

Furthermore, to quantitatively inspect the developed model, different statistical criteria containing mean absolute error (MAE), root mean square error (RMSE), coefficient of determination (R^2 or R -squared) and mean absolute percentage error (MAPE) are utilized. These criteria are defined as:

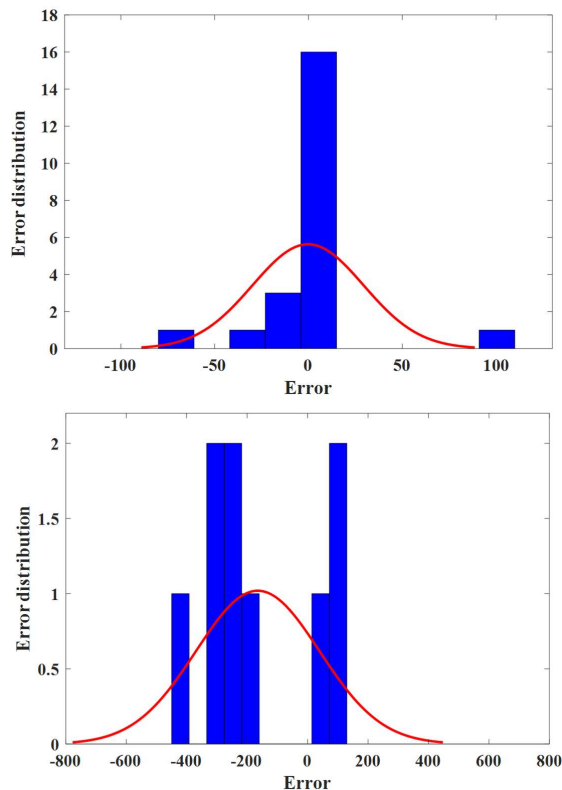


Fig. 12. Error histogram for training and testing sections.

$$RMSE = \sqrt{\frac{1}{n} \sum_{i=1}^n (O_A - O_P)^2} \quad (23)$$

$$MAE = \frac{1}{n} \sum_{i=1}^n |O_A - O_P| \quad (24)$$

$$R^2 = \frac{[\sum_{i=1}^n (O_A - \bar{O}_A)(O_P - \bar{O}_P)]^2}{[\sum_{i=1}^n (O_A - \bar{O}_A)][\sum_{i=1}^n (O_P - \bar{O}_P)]} \quad (25)$$

$$MAPE = \frac{100\%}{n} \sum_{i=1}^n \left| \frac{O_A - O_P}{O_A} \right| \quad (26)$$

where O_A is the measured output value for the i -th data, O_P is the approximated output by the ANFIS for the i -th sample, \bar{O}_A is the mean of measured data and \bar{O}_P is the mean of predicted data. To examine the model accurateness,

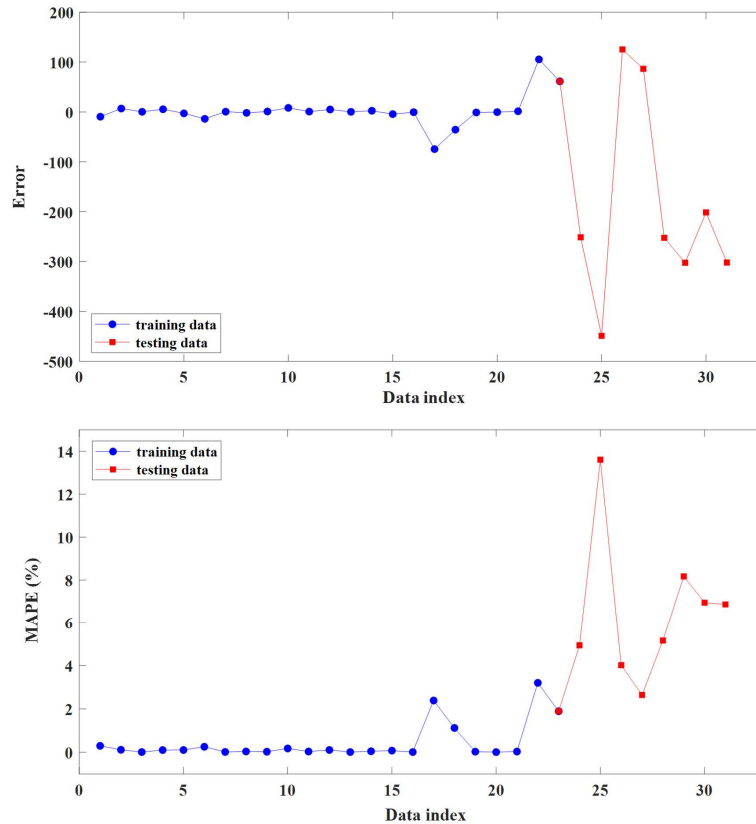


Fig. 13. Error and mean absolute percentage error for the training and testing sections.

the above-mentioned criteria are independently computed for training and test sections, as shown in Table 5.

Table 5. RMSE, MAE, R^2 and MAPE criteria for TSS of welded joints

	RMSE	MAE	R^2	MAPE (%)
Train	29	13	0.99	0.37
Test	253	225	0.96	6.02

From the listed values in Table 5, it becomes clear that the ANFIS has been notably successful in predicting the TSS. The criteria RMSE and MAE are small, while they alone are not appropriate for model evaluation. Next, R^2 and MAPE criteria that determine the amount of error relative to the number of data are used. The coefficient of determination, R^2 , is so close to one, indicating the high accuracy of the model. The percentage errors of MAPE in the training section are 0.37%. Furthermore, the MAPE in the test section are 6.02%. It can be seen here that the ANFIS error in the test section is relatively greater compared with the

training section. This is completely expected as in the training section, all training data (70% of all data) are used, and the model has been developed in such a way that the network outputs completely match the utilized data, whereas the network test is carried out based on the test data (the remaining 30% of the data) and this data is not used in the network training section. Thus, due to the existence of error in empirical data, this amount of error in estimation is to be expected.

3.2. Analysis of the effects of input parameters on TSS based on sensitivity analysis

3.2.1. The effect of welding current

It can be concluded from Fig. 14 that increase in the welding current leads to an increase in the TSS because the generated heat in the welding zone and consequently the weld nugget rises. It should be noted that larger weld nugget diameter leads to higher TSS [21].

3.2.2. The effect of welding cycle

It can be proved from Fig. 15 that the TSS is increased by enlarging the welding.

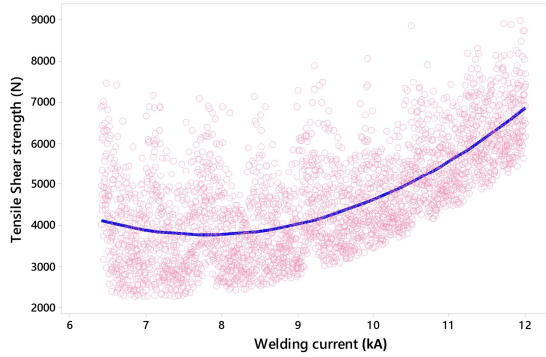


Fig. 14. Effect of welding current on TSS of spot welds.

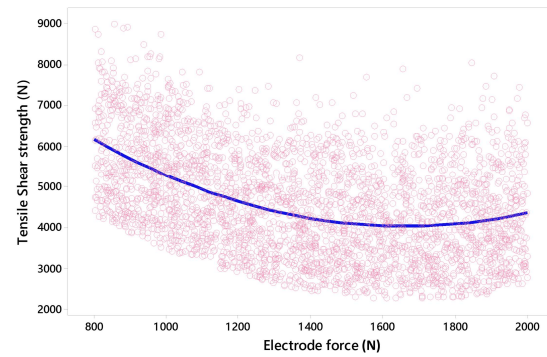


Fig. 16. Effect of electrode force on TSS of spot welds.

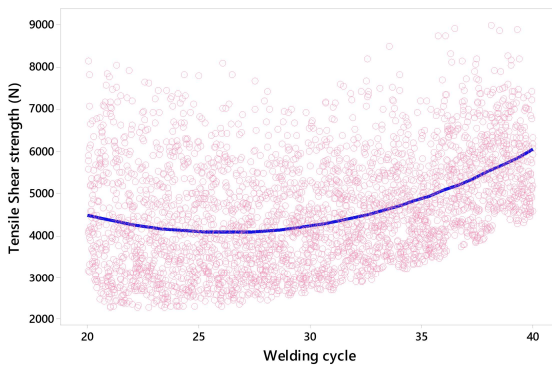


Fig. 15. Effect of welding cycle on TSS of spot welds.

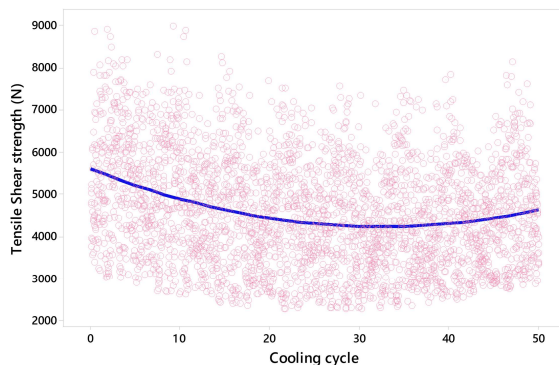


Fig. 17. Effect of cooling cycle on TSS of spot welds.

3.2.3. Effect of electrode force

As shown in Fig. 16, the TSS of the joints decreases by increasing the electrode force due to decreasing the electrical resistance at the welding area and then reducing the heat energy. In addition, more electrode force leads to a reduction in the weld nugget diameter, and consequently a reduction in the weld nugget diameter reduces the amount of joint strength [22].

3.2.4. Effect of cooling cycle

In Fig. 17, the effect of cooling cycle on TSS can be seen and it is proved the TSS will be decreased by increasing the cooling cycle. The reason is as the carbon content of AISI 1060 is high, increasing the cycle leads to an increase in the risk of brittle microstructure in the welded joint. In addition, increasing the cooling cycle leads to an increase in primary grain size that then encourages the martensite formation at weld region [23].

3.3. Sobol sensitivity analysis of tensile shear of RSW joints

Using the Simlab software, which simultaneously changes the input parameters for evaluating their effects on output [19], the result of Sobol sensitivity analysis for the TSS is shown in Fig. 18. It is concluded that welding current, electrode force, welding cycle and cooling cycle are the most effective parameters that, respectively, strengthen the joints.

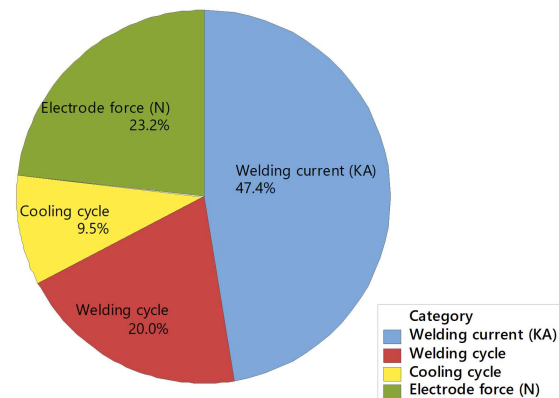


Fig. 18. The diagram of effectiveness of input parameters on TSS of RSW joints.

4. Conclusion

In this paper, RSW of AISI 1060 steel sheets were experimentally investigated. The effects of welding current, welding cycle, electrode force and cooling cycle were modeled and predicted by ANFIS-GWO and Sobol sensitivity analysis methods. The following results were obtained:

1. Welding current, welding cycle, cooling cycle and electrode force, their squares and some interactions influenced the strength of the joints.

2. It was concluded that increase in the welding current leads to a rise in the TSS given the rise in the generated heat in the welding zone and consequently the weld nugget.

3. It was proved that the TSS is increased by increasing the welding cycle because of a rise in the generated heat in the welding zone and consequently enlarging the weld nugget diameter.

4. The TSS of the joints decreases by increasing the electrode force due to a fall in the electrical resistance at welding area and then reducing the heat energy. In addition, more electrode force leads to a reduction in the weld nugget diameter, and consequently a reduction in the weld nugget diameter reduces the amount of joint strength.

5. It was proved that the TSS will decrease by increasing the cooling cycle. The reason was as the carbon content of AISI 1060 is high, increasing the cycle leads to rise in the risk of brittle microstructure in the welded joint.

6. The results showed that the ANFIS network was very suitable in predicting TSS based on variation in RSW process parameters and the coefficients of determination and mean absolute percentage error confirmed the effectiveness of this method.

7. It was concluded from Sobol sensitivity analysis method that welding current, electrode force, welding cycle and cooling cycle are the most effective parameters on the strength of joints, respectively.

Compliance with Ethical Standards

Authors hereby announce that no part of this study was funded by any institutions and /or organizations. The authors also acknowledge no conflict of interests.

5. References

- [1] Ó. Martín, P. De Tiedra, and M. San-Juan, Combined effect of resistance spot welding and precipitation hardening on tensile shear load bearing capacity of A286 superalloy, *Materials Science and Engineering: A*, 2017. 688 (2017) 309-314.
- [2] J. Bi, J. Song, Q. Wei, Y. Zhang, Y. Li, Z. Luo, Characteristics of shunting in resistance spot welding for dissimilar unequal-thickness aluminum alloys under large thickness ratio, *Materials & Design*, 101 (2016) 226-235.
- [3] M. Safari, H. Mostaan, H. Yadeghari Kh., D. Asgari, Effects of process parameters on tensile-shear strength and failure mode of resistance spot welds of AISI 201 stainless steel, *The International Journal of Advanced Manufacturing Technology*, 89(5-8) (2017) 1853-1863.
- [4] M. Safari, H. Mostaan, Experimental investigation of the effects of process parameters on the strength of eutectoid steel (AISI 1075) sheet resistance spot welds, *Metallurgical Research & Technology*, 113(3) (2016) 305.
- [5] M. Safari, H. Mostaan, A. Ghaderi, Dissimilar resistance spot welding of AISI 304 to AISI 409 stainless steels: mechanical properties and microstructural evolutions, *Metallurgical Research & Technology*, 115(6) (2018) 610.
- [6] M. Safari, J. Joudaki, Experimental investigation of resistance spot welding of ultrathin IF steel sheets. *International Journal of Iron & Steel Society of Iran*, 16(1) (2019) 51-57.
- [7] R. Kumar, J.S. Chohan, R. Goyal, P. Chauhan, Impact of process parameters of resistance spot welding on mechanical properties and micro hardness of stainless steel 304 weldments, *International Journal of Structural Integrity*, 2020.
- [8] T. Chen, Z. Ling, M. Wang, L. Kong, Effect of a slightly concave electrode on resistance spot welding of Q&P1180 steel, *Journal of Materials Processing Technology*, 285 (2020) 116797.
- [9] D. Zhao, M. Ivanov, Y. Wang, D. Liang, W. Du, Multi-objective optimization of the resistance spot welding process using a hybrid approach, *Journal of Intelligent Manufacturing*, (2020) 1-16.

- [10] Y.J. Xia, Z.W. Su, Y.B. Li, L. Zhou, Y. Shen, Online quantitative evaluation of expulsion in resistance spot welding, *Journal of Manufacturing Processes*, 46 (2019) 34-43.
- [11] J.H. Ordoñez, R.R. Ambriz, C. García, G. Plascencia, D. Jaramillo, Overloading effect on the fatigue strength in resistance spot welding joints of a DP980 steel, *International Journal of Fatigue*, 121 (2019) 163-171.
- [12] J. Valera, V. Miguel, A. Martínez, J. Naranjo, M. Cañas, Optimization of electrical parameters in resistance spot welding of dissimilar joints of micro-alloyed steels TRIP sheets, *Procedia Manufacturing*, 13 (2017) 291-298.
- [13] K. Vignesh, A.E. Perumal, P. Velmurugan, Optimization of resistance spot welding process parameters and microstructural examination for dissimilar welding of AISI 316L austenitic stainless steel and 2205 duplex stainless steel, *The International Journal of Advanced Manufacturing Technology*, 93(1) (2017) 455-465.
- [14] X. Wan, Y. Wang, D. Zhao, Y. Huang, A comparison of two types of neural network for weld quality prediction in small scale resistance spot welding, *Mechanical Systems and Signal Processing*, 93 (2017) 634-644.
- [15] Y. Cho, S. Rhee, Quality estimation of resistance spot welding by using pattern recognition with neural networks, *IEEE Transactions on Instrumentation and Measurement*, 53(2) (2004) 330-334.
- [16] B.N. Panda, M.R. Babhubalendruni, B.B. Biswal, D.S. Rajput, Application of artificial intelligence methods to spot welding of commercial aluminum sheets (BS 1050), In Proceedings of Fourth International Conference on Soft Computing for Problem Solving. Springer, New Delhi, 2015, pp. 21-32.
- [17] J.S. Jang, ANFIS: adaptive-network-based fuzzy inference system, *IEEE transactions on systems, man, and cybernetics*, 23(3) (1993) 665-685.
- [18] S. Mirjalili, S.M. Mirjalili, A. Lewis, Grey wolf optimizer, *Advances in Engineering Software*, 69 (2014) 46-61.
- [19] I.M. Sobol, Sensitivity analysis for non-linear mathematical models, *Mathematical Modelling and Computational Experiment*, 1 (1993) 407-414.
- [20] D.C. Montgomery, Design and analysis of experiments, John Wiley & sons, 2017.
- [21] Y. Kaya, N. Kahraman, The effects of electrode force, welding current and welding time on the resistance spot weldability of pure titanium, *The International Journal of Advanced Manufacturing Technology*, 60(1-4) (2012) 127-134.
- [22] K. Zhou, L. Cai, Study on effect of electrode force on resistance spot welding process, *Journal of applied physics*, 116(8) (2014) 084902.
- [23] M. Pouranvari, S. Marashi, Critical review of automotive steels spot welding: process, structure and properties, *Science and Technology of Welding and Joining*, 18(5) (2013) 361-403.